Journal of proteome research

Article

pubs.acs.org/jpr

Synaptic Proteome Changes in a DNA Repair Deficient *Ercc1* Mouse Model of Accelerated Aging

Marlene J. Végh,[†] Monique C. de Waard,[‡] Ingrid van der Pluijm,[‡] Yanto Ridwan,[‡] Marion J. M. Sassen,[†] Pim van Nierop,[†] Roel C. van der Schors,[†] Ka Wan Li,[†] Jan H. J. Hoeijmakers,[‡] August B. Smit,[†,§] and Ronald E. van Kesteren*[,†,§]

[†]Center for Neurogenomics and Cognitive Research, Neuroscience Campus Amsterdam, VU University, De Boelelaan 1085, 1081 HV Amsterdam, The Netherlands

[‡]CGC Department of Genetics, Erasmus Medical Center, Dr. Molewaterplein 50, 3015 GE Rotterdam, The Netherlands

Supporting Information

ABSTRACT: Cognitive decline is one of the earliest hallmarks of both normal and pathological brain aging. Here we used *Ercc1* mutant mice, which are impaired in multiple DNA repair systems and consequently show accelerated aging and progressive memory deficits, to identify changes in the levels of hippocampal synaptic proteins that potentially underlie these age-dependent deficits. Aged *Ercc1* mutant mice show normal gross hippocampal dendritic morphology and synapse numbers, and *Ercc1* mutant hippocampal neurons displayed normal outgrowth and synapse formation *in vitro*. However, using isobaric tag for relative and absolute quantification (iTRAQ) of hippocampal synaptic proteins at two different ages, postnatal days 28 and 112, we observed a progressive decrease in synaptic ionotropic glutamate receptor levels and increased levels of G-proteins and of cell adhesion proteins. These together may cause long-term changes in synapse function. In addition, we observed a downregulation of mitochondrial proteins and concomitant upregulation of Na,K-ATPase subunits, which might compensate for reduced mitochondrial activity. Thus, our findings show that under conditions of apparent intact neuronal connectivity, levels of specific synaptic proteins are already affected during the early stages of DNA damage-induced aging, which might contribute to age-dependent cognitive decline.

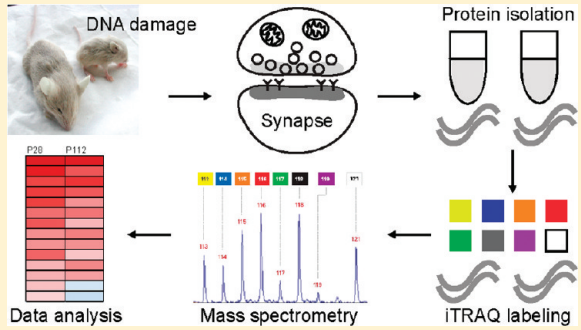

KEYWORDS: *aging, DNA repair, proteomics, iTRAQ, hippocampus, synapse*

INTRODUCTION

Impaired memory function is one of the earliest cognitive signs of both normal and pathological brain aging. This decline can be partly explained by early changes in synaptic transmission and/or plasticity, especially in brain areas related to learning and memory, such as the hippocampus. Neuronal and synaptic dysfunction precede age-related synapse loss and neuronal degeneration and occur long before, or even in the absence of, cell death in humans[1] as well as in animals.[2−4] Moreover, in aged animals subtle changes in synaptic function appear to contribute to alterations in plasticity.[5] How synaptic dysfunction disrupts neuronal network dynamics of aged neurons and ultimately leads to behavioral deficits and cognitive decline is still unknown. Molecular and functional analysis of aging synapses may therefore provide important clues as to how age-related cognitive decline is triggered and how it may eventually be treated.

DNA damage plays an important role in aging.[6] Unrepaired DNA damage triggers a complex DNA damage response and may give rise to epigenetic changes,[7] gene silencing, and specific changes in gene expression.[8,9] In addition, persistent DNA injury may interfere with transcription and/or replication, triggering cell dysfunction, cell death, or permanent cell cycle arrest. These processes are considered to be important causative factors in aging. This is reflected in rare inherited disorders named segmental progeroid syndromes, in which genome maintenance is compromised and many features of aging are accelerated.[10−12] Natural aging is however highly variable in its onset and progression, and genetically modified mice in which DNA damage is induced or DNA repair is impaired are therefore attractive models to study the biology of aging.[13] Here, we use *Ercc1* mutant mice, which have a defective DNA repair mechanism and, as a consequence of unrepaired DNA damage, have a progeroid phenotype. Ercc1 forms a complex with the xeroderma pigmentosum group F protein (XPF) and acts as nuclease in the nucleotide excision repair (NER) pathway.[14] In addition, it is also involved in interstrand cross-link repair and double-strand break (DSB) repair.[15−19] *Ercc1* knockout (*Ercc1*$^{-/-}$) mice develop a severe and accelerated aging phenotype, including early cessation of growth, ataxia, and cachexia, and die prematurely at an age of

Received: October 31, 2011
Published: January 30, 2012

3−8 weeks.[20−22] *Ercc1*$^{\Delta/-}$ mice on the other hand have a knockout mutation in one allele of the *Ercc1* gene and a premature stop codon in the other allele, resulting in a truncated Ercc1 protein, which lacks the last 7 amino acids.[21] Therefore, *Ercc1*$^{\Delta/-}$ mice have a milder phenotype compared to *Ercc1*$^{-/-}$ mice and die at an age of 4−6 months. They display many signs of accelerated aging, including motor neuron degeneration,[23] changes in metabolism,[24] and age-dependent impairments in synaptic plasticity and learning behavior.[25]

Here we took advantage of the highly predictive accelerated aging pattern observed in *Ercc1* mutant mice in order to robustly identify DNA damage-induced age-related changes in hippocampal synaptic protein composition that may be difficult to detect under normal aging conditions. After having established that *Ercc1* mutant mice have no apparent features of affected hippocampal neuronal connectivity, including synapse numbers, we used direct approaches to quantitatively address the synaptic proteome. Specifically, we assessed biochemically enriched synaptosome fractions and performed proteomic analyses using isobaric tag for relative and absolute quantfication (iTRAQ) followed by tandem mass spectrometry. This approach identified proteins whose levels are altered in 4- and 16-week-old *Ercc1* mutant mice and are discussed in the context of age-related cognitive decline.

EXPERIMENTAL SECTION

Ercc1 Mutant Mice

The generation of *Ercc1*$^{-/-}$ and *Ercc1*$^{\Delta/-}$ alleles has been previously described.[21] *Ercc1*$^{\Delta/-}$ mice were obtained by crossing *Ercc1*$^{+/-}$ with *Ercc1*$^{\Delta/+}$ mice of C57Bl6J and FVB backgrounds, respectively, and vice versa, to yield *Ercc1*$^{\Delta/-}$ with an F1 C57Bl6J/FVB hybrid background. *Ercc1*$^{-/-}$ mice were obtained by crossing *Ercc1*$^{+/-}$ with *Ercc1*$^{+/-}$ mice of C57Bl6J and FVB backgrounds to yield *Ercc1*$^{-/-}$ with an F1 C57Bl6J/FVB hybrid background. Wildtype littermates were used as controls. Breeding was performed in accordance with the Principles of Laboratory Animal Care (NIH publication no. 86-23) and with the guidelines approved by the Erasmus University Animal Care Committee. All animal experiments were approved by the Animal Users Care Committee of the VU University Amsterdam (protocol MCN 08-06).

Primary Hippocampal Cultures

Hippocampi were dissected from E18 *Ercc1*$^{-/-}$, *Ercc1*$^{\Delta/-}$, and wildtype embryos and collected in Hanks balanced salts solution (HBSS; Sigma-Aldrich, St. Louis, MO), buffered with 7 mM HEPES (Invitrogen, Carlsbad, CA, USA). Hippocampi were incubated for 30 min in HBBS containing 0.25% trypsin (Invitrogen) at 37 °C. After washing, neurons were triturated using fire-polished Pasteur pipettes, counted, and plated in Neurobasal medium supplemented with 2% B-27, 1.8% HEPES, 1% glutamax, 1% Pen Strep (all from Invitrogen) and 0.2% 14.3 mM β-mercapto-ethanol. Cells were plated in 96-well plates (Cellstar, Greiner Bio-One, Frickenhausen, Germany) that were previously coated with poly-D-lysine (Sigma-Aldrich) and 5% heat-inactivated horse serum (Invitrogen). Neurons were plated at a seeding density of 830 cells/mm^2 and cultured at 37 °C/5% CO_2 for up to 15 days. Half of the medium was replaced with fresh medium every week.

Immunofluorescence and High-Content Screening

Neurons were fixed for 12 min using 4% paraformaldehyde and 4% saccharose in PBS (pH 7.4), washed with PBS, permeabilized with 0.25% Triton X-100 in PBS for 4 min, and blocked for 1 h in 1% BSA in PBS. Neurons were stained with chicken anti-MAP2 (Abcam, Cambridge, U.K.; 1:5,000) and anti-Synapsin I (Millipore, Billerica, MA, USA; 1:1,000) overnight at 4 °C. Antigens were visualized using Alexa Fluor 488 and 568 (Invitrogen; 1:400) incubated for 2 h at room temperature. Neurite outgrowth and synapse formation were quantified using a Cellomics ArrayScan HCS Reader and the Cellomics Neuronal Profiling 3.5 bioapplication (Thermo Scientific, Pittsburgh, PA, USA). In these experiments, Ercc1$^{-/-}$ (n = 6) and wildtype (n = 6) neurons were used, and per experiment 400−1,200 cells were analyzed and neuron counts, neurite lengths, and synapse numbers were determined. Significance was calculated using univariate analyses of variance (ANOVA).

Immunohisotchemistry

Mice were intracardially perfused with ice-cold paraformaldehyde (4% PFA in PBS, pH 7.4). Brains were removed, postfixed, embedded in paraffin, microtome-sectioned at 6 μm, and stained with anti-MAP2 (Millipore; 1:2,000). As secondary antibody Dylight 549 (Jackson ImmunoResearch, West Grove, PA, USA; 1:400) was used. Confocal microscopy was performed using a Carl Zeiss LSM 510 (Zeiss, Germany) at 40x magnification.

Golgi-Cox Staining

Ercc1$^{\Delta/-}$ (n = 3) and wildtype (n = 3) mice were intracardially perfused with ice-cold paraformaldehyde (4% in PBS, pH 7.4). Brains were removed, postfixed and Golgi-Cox staining was performed using the FD Rapid GolgiStain Kit (FD NeuroTechnologies, Ellicott City, MD, USA). After staining, brains were microtome-sectioned at 100 μm. Neurons were photographed using a Carl Zeiss LSM 510 meta laser scanner at 63x magnification and Z-stacks were generated using Carl Zeiss LSM Image Browser 4.2 software. Z-stacks were used in ImageJ 1.44 g software (NIH, Bethesda, MD, USA) for synapse counting and dendrite length measurements. To keep the counting procedure consistent, we only counted spines of which the spine heads clearly protruded laterally from the dendritic shafts. Spine densities were calculated by dividing the total number of spines by the total dendritic length.

Synaptosome Isolation and Sample Preparation

Hippocampi were dissected, frozen, and stored at −80 °C until protein isolation. Synaptosomes were isolated from hippocampi of *Ercc1*$^{\Delta/-}$ mice and wildtype littermates at two different ages, 4 weeks (P28) and 16 weeks (P112), as described previously[26,27] with minor modifications. Eight animals were used per genotype per time point. In order to obtain sufficient amounts of protein, hippocampi of two mice were pooled, resulting in four biological replicates per genotype per time point (n = 4 per genotype, per time point). In brief, pooled samples were homogenized in ice-cold 0.32 M sucrose buffer with 5 mM HEPES at pH 7.4 and protease inhibitor (Roche) and centrifuged at 1000 × g for 10 min at 4 °C to remove debris. Supernatant was loaded on top of a discontinuous sucrose gradient consisting of 0.85 and 1.2 M sucrose. After ultracentrifugation at 110,000 × g for 2 h at 4 °C, the synaptosome fraction was collected at the interface of 0.85 and 1.2 M sucrose, resuspended, and pelleted by ultracentrifugation

dx.doi.org/10.1021/pr201203m | J. Proteome Res. 2012, 11, 1855−1867

at 80,000 × *g* for 30 min at 4 °C, after which the material was redissolved in 5 mM HEPES. Protein concentrations were determined using a Bradford assay (Bio-Rad, Hercules, CA, USA). For each sample, 75 μg of protein was transferred to a fresh tube and dried in a SpeedVac overnight.

Protein Digestion and iTRAQ Labeling

Per sample, 75 μg synaptosome proteins were dissolved in 0.85% RapiGest (Waters Associates, Milford, MA, USA), alkylated with methyl methanethiosulfonate, and digested with trypsin (sequencing grade; Promega, Madison, WI, USA) as described.[27,28] In each iTRAQ experiment, four wildtype samples were labeled respectively with iTRAQ reagents 113−116, and four Ercc1$^{\Delta/-}$ samples with iTRAQ reagents 117−119 and 121. To accommodate four biological replicates in each experiment (P28 and P112), a total of two 8-plex iTRAQ experiments was performed (Supplemental Figure S1).

Two-dimensional liquid chromatography (2DLC)

The lyophilized iTRAQ labeled samples were separated in the first dimension by strong cation exchange column (2.1 × 150 mm polysulfethyl A column, PolyLC), and the in second dimension on an analytical capillary reverse phase C18 column (150 mm × 100 μm i.d. column) at 400 nL/min using the LC-Packing Ultimate system. The peptides were separated using a linear increase in concentration of acetonitrile from 4% to 28% in 75 min, to 36% in 7 min, and finally to 72% in 2 min. The eluent was mixed with matrix (7 mg of recrystallized α-cyano-hydroxycinnaminic acid in 1 mL of 50% acetronitrile, 0.1% trifluoroacetic acid, 10 mM ammonium dicitrate) and delivered at a flow rate of 1.5 μL/min and deposited onto an Applied Biosystems matrix-assisted laser desorption ionization plated by means of a robot (Probot, Dionex) once every 15 s for a total of 384 spots.

MALDI MS/MS

Samples were analyzed on an ABI 4800 proteomics analyzer (Applied Biosystems, Forster City, CA). Peptide collision-induced dissociation was performed at 2 kV, and the collision gas was air. MS/MS spectra were collected from 2500 laser shots. Peptides with signal-to-noise ratios over 50 at the MS mode were selected for MS/MS analysis, at a maximum of 30 MS/MS per spot. The precursor mass window was set to a relative resolution of 200. Peaklists were extracted from the instrument database using TS2Mascot software (MatrixScience).

Protein Identification

Protein identification and quantification are described in detail in ref 29. To annotate spectra, Mascot (MatrixScience) searches were performed against the Swissprot database (release January 2009; 16,028 mouse entries) and against the larger but more redundant NCBI database (release January 2009; 140,210 mouse entries) using the GPS Explorer software (version 3.6, Applied Biosystems). MS/MS spectra were searched with trypsin specificity and fixed iTRAQ modifications on lysine residues and N-termini of the peptides and methylthio modifications on cysteine residues. Oxidation on methionine residues was allowed as a variable modification. Mass tolerance was 150 ppm for precursor ions and 0.5 Da for fragment ions, while allowing a single site of miscleavage. The false discovery rate (FDR) for peptides identification was calculated using a randomized database (P28: 0.028 and 0.025; P112: 0.027 and 0.027 for NCBI and SwissProt respectively). Protein redundancy in the result files was removed by clustering the precursor protein sequences at a threshold of 90% sequence similarity over 85% of the sequence length. Subsequently all peptides were matched against the protein clusters and only those peptides were included that mapped unique to one protein. Proteins were considered for quantification if at least three unique peptide had a confidence interval of ≥95%, and at least three peptides were identified in both experiments (P28 and P112; stringent selection criteria), or at least three peptides were identified in one experiment and at least one peptide in the other (relaxed selection criteria).

Protein Quantification and Identification of Differentially Expressed Proteins

iTRAQ areas (m/z 113−121) were extracted from raw spectra and corrected for isotopic overlap using GPS explorer. Peptides with iTRAQ signature peaks of less than 1500 were not considered for quantification. To compensate for the possible variations in the starting amounts of the samples, the individual peak areas of each iTRAQ signature peak were log transformed to yield a normal distribution and normalized to the mean peak area of every sample. Protein abundances in every experiment were determined by taking the average normalized standardized iTRAQ peak area of all unique peptides annotated to a protein. Finally, the standardized protein means (four mutant and four wildtype in each experiment) were used to calculate the average difference between wildtype and mutant mice. To assess whether differences had occurred by chance or could be deemed significant, we calculated permutation-derived false discovery rates (FDR), using Significance Analysis of Microarrays (SAM)[30] as implemented in the Multi Experiment Viewer software (MeV, version 4.6.1).[30,31] Conventional *t*-tests or fold change alone do not take into account the effect of multiple testing and tend to overestimate the number of differentially regulated proteins. SAM on the other hand is a data resampling-based method and creates randomized data distributions in order to estimate false positive rates.[30] In contrast to conventional multiple testing correction methods, SAM is more adaptive to different biological experiments that may have asymmetrical distribution of differential protein expression profiles. It was previously demonstrated that SAM can be successfully applied to proteomics data.[32−36] The SAM *q*-values reflect for each protein the number of empirically determined false-positives at the significance level of the respective protein. The false discovery rate (FDR) levels in our results thus hold information about individual proteins and should not be interpreted as a global FDR. Changes in protein expression are considered to be significant when the FDR is <10%.

Functional Protein Group Analysis

All quantified proteins were assigned to one of 17 functional synaptic protein groups as previously defined.[37,38] Up- and downregulated proteins at each time point (P28 and P112) were separately tested for overrepresentation of functional protein groups using a Fisher's exact test.

Immunoblotting

Western blot analysis was performed on six independent synaptosome protein extracts, i.e., the four samples that were used in the iTRAQ experiment plus two independent samples derived from two animals each. Of each sample, 2.5 μg protein was mixed with SDS sample buffer and heated to 90 °C for 5 min. Proteins were separated on a Criterion XT Precast Gel

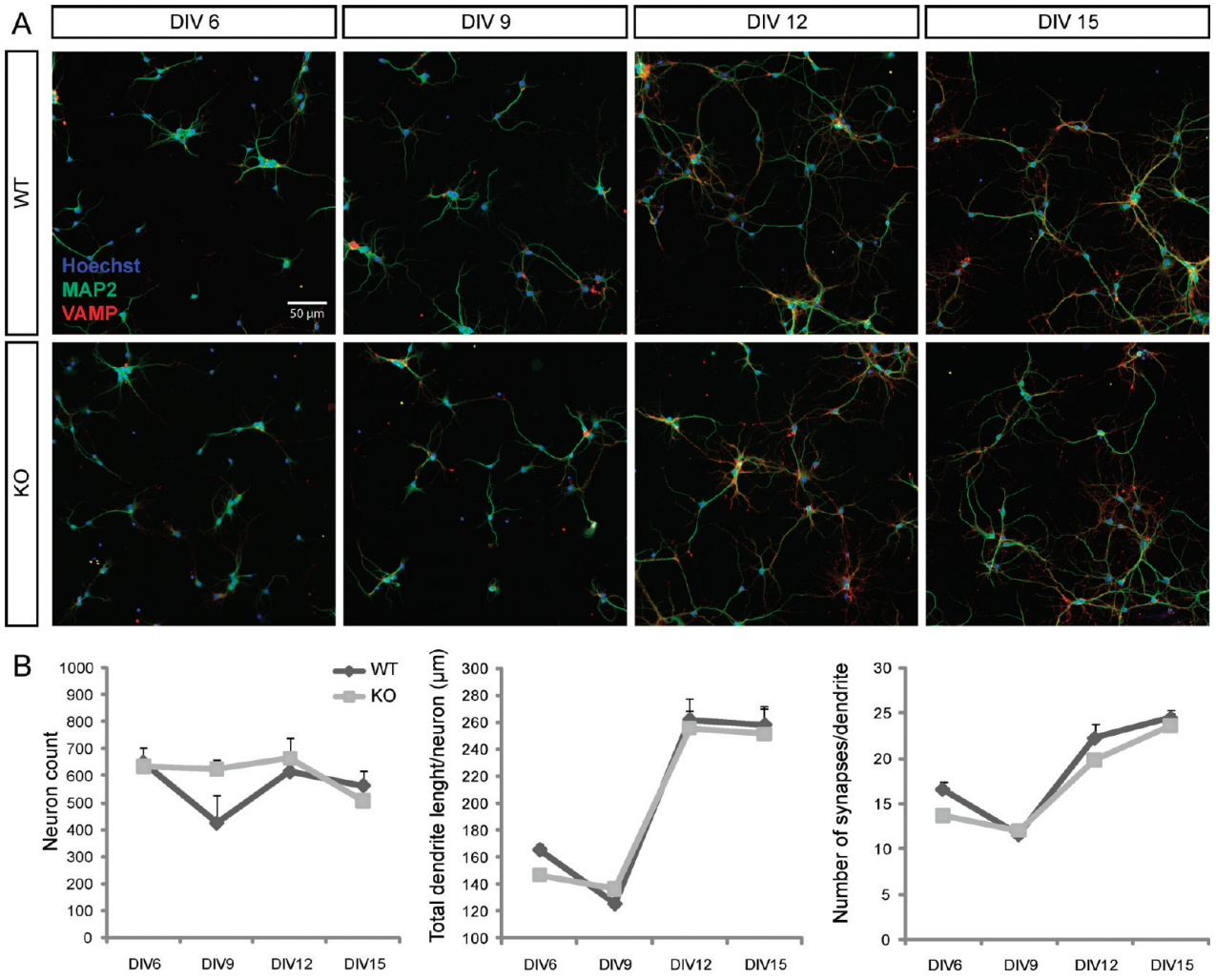

Figure 1. *Ercc1*$^{-/-}$ hippocampal neurons display normal outgrowth and synapse formation *in vitro*. (A) E18 primary hippocampal neurons of *Ercc1*$^{-/-}$ (KO) mice and wildtype (WT) littermates were fixed at DIV6, DIV9, DIV12, and DIV15 and co-stained with a nuclear marker (Hoechst), a dendritic marker (MAP2), and a presynaptic vesicle marker (VAMP). (B) Total cell numbers were stable over time. Dendrite length and the number of synapses per dendrite increased over time, indicating maturation of the neuronal network. No differences in network development were observed between *Ercc1*$^{-/-}$ mice and wildtype littermates.

(4−12% Bis-Tris; Bio-Rad) in a Criterion Cell Electrophoresis System (Bio-Rad) and electroblotted onto PVDF membrane overnight at 4 °C. After blocking with 5% nonfat dry milk in TBS-T (TBS plus 0.5% Tween) for 1 h, blots were incubated with primary antibodies, followed by an alkaline phosphatase-conjugated secondary antibody (Dako, Glostrup, Denmark; 1:10,000). The following antibodies were used: anti-PSD95 (NeuroMab, Davis, CA, USA; 1:5,000), anti-UQCRC2 (Abcam; 1:500), anti-GAP43 (GenScript, New Jersey, NJ, USA; 1:2,000), anti-NCAM (Hybrdoma Bank, Iowa City, IA, USA; 1:2,000), anti-ATP1B2 (GenScript; 1:2,000), anti-CamKIIa (GenScript; 1:1,000), and anti-GluA1 (GenScript; 1:1,000). Blots were incubated with ECF substrate (GE Healthcare, Pollards Wood, U.K.), scanned with a FLA 5000 instrument (Fujifilm) and analyzed with Quantity One software (Bio-Rad) using background correction. To correct for differences in sample input, half of the same gel was stained with Coomassie blue and scanned, and the densitometric values were used for normalization.[28,36] Significance was determined using a Student's *t*-test (1-tailed, independent samples).

RESULTS

Ercc1$^{-/-}$ Hippocampal Neurons Display Normal Outgrowth and Synapse Formation *in Vitro*

Ercc1 mutant mice are normal at birth but soon develop a severe and accelerated aging phenotype. To investigate whether neurons in the central nervous system are normal at birth and are not functionally impaired due to their inability to repair DNA during embryonic development, we isolated E18 primary hippocampal neurons from *Ercc1*$^{-/-}$ mice and tested whether these neurons are capable of normal dendrite outgrowth and synapse formation *in vitro* compared to wildtype neurons. Neurons were cultured, fixed at DIV6, DIV9, DIV12, and DIV15, and co-stained with a nuclear marker (Hoechst), a dendritic marker (MAP2), and a presynaptic vesicle marker (VAMP) (Figure 1A). Dendrite outgrowth and synapse formation were quantified using automated high-content microscopy. No significant differences in dendrite outgrowth and synapse formation were observed between *Ercc1*$^{-/-}$ and wildtype neurons (Figure 1B), indicating that neuronal network development of *Ercc1*$^{-/-}$ neurons proceeds normally *in vitro*. Moreover, the number of neurons remained the same over

dx.doi.org/10.1021/pr201203m | *J. Proteome Res.* 2012, 11, 1855−1867

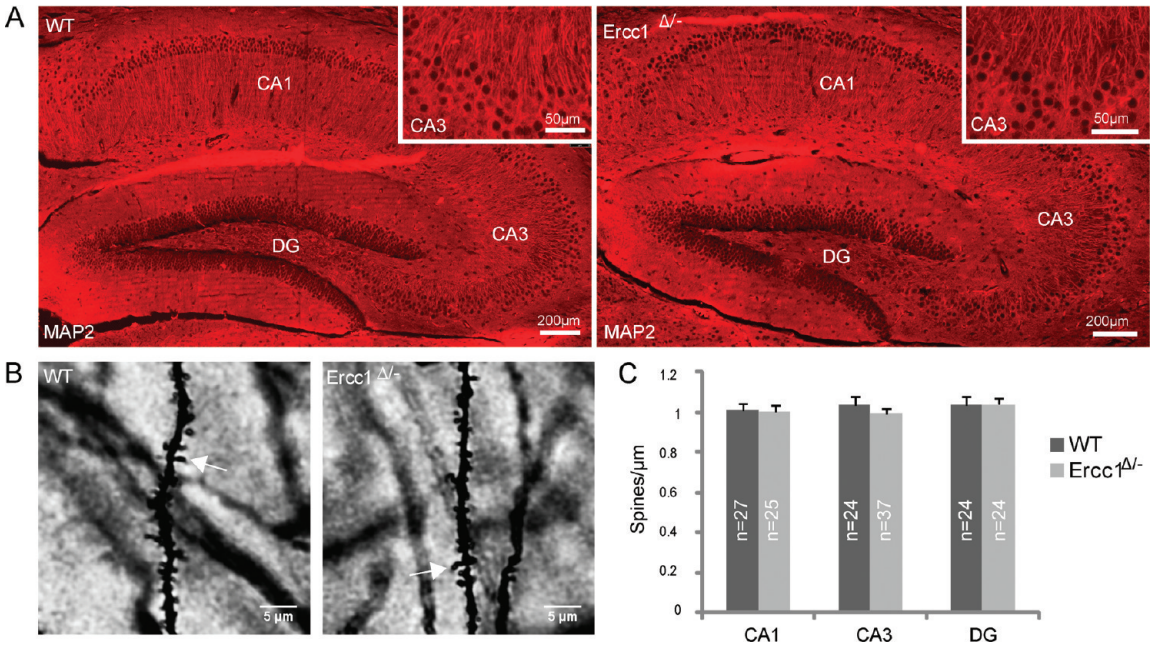

Figure 2. *Ercc1*$^{\Delta/-}$ mice have normal hippocampal synapse numbers at 16 weeks of age. (A) MAP2 immunohistochemistry on hippocampal sections revealed no differences between *Ercc1*$^{\Delta/-}$ mice and wildtype control mice in the distribution or the staining intensity of the dendritic marker MAP2. (B) Representative images of Golgi-Cox-stained sections of the hippocampal CA1 region. Spines were counted as synapses when spine heads were clearly visible outside the dendritic shaft region (arrowheads indicates examples valid spine profiles). (C) Quantification of dendritic spine densities in the CA1, CA3 and dentate gyrus (DG) regions of the hippocampus shows no differences between *Ercc1*$^{\Delta/-}$ mice and wildtype littermates. *N*-numbers represent the numbers of dendrites included in the spine counts.

time, indicating that the *Ercc1*$^{-/-}$ repair defect did not cause increased cell death under normal conditions. These findings show that *Ercc1* mutant hippocampal neurons have no apparent developmental impairments that might account for the age-related deficits observed postnatally. Interestingly, when neurons were exposed to rotenone in order to inhibit mitochondrial electron transport,[39] we observed a significant reduction in the viability of *Ercc1*$^{-/-}$ neurons compared to wildtype neurons, suggesting impaired mitochondrial function in *Ercc1*$^{-/-}$ neurons and increased susceptibility to oxidative stress (data not shown).

Ercc1$^{\Delta/-}$ Mice Have Normal Hippocampal Synapse Densities at 16 Weeks of Age

To determine whether synapse numbers are affected in *Ercc1* mutant mice *in vivo*, we performed immunohistochemistry on hippocampal sections of *Ercc1*$^{\Delta/-}$ and wildtype mice at P112. We used *Ercc1*$^{\Delta/-}$ mice in these and in all following experiments, as they allow a temporal window of 16 weeks to study age-related synaptic changes, whereas *Ercc1*$^{-/-}$ mice die at an age of 4 weeks on average. No differences were observed between hippocampal sections of *Ercc1*$^{\Delta/-}$ mice and wildtype control mice in the distribution or in the staining intensity of the dendritic marker MAP2 (Figure 2A); both the dendritic layers and the cell body layers have a normal gross morphological appearance. In addition, we performed Golgi-Cox staining and quantified synapses in all regions of the hippocampus of *Ercc1*$^{\Delta/-}$ mice and of wildtype controls. No differences were observed in the density of dendritic spines in any region of the hippocampus (Figure 2B and C). Together, these findings show that hippocampal synapse numbers are normal in 16-week-old *Ercc1*$^{\Delta/-}$ mice and are consistent with earlier reports showing that hippocampal morphology and cell numbers are normal in aged *Ercc1*$^{\Delta/-}$ mice.[25]

Ercc1$^{\Delta/-}$ Mice Show Age-Related Changes in Hippocampal Synapse Protein Composition

After having established normal growth, synapse formation, synapse numbers, and connectivity of hippocampal neurons, both *in vitro* and *in vivo*, we continued to investigate age-dependent changes in the molecular composition of the hippocampal synapses. Specifically, we performed 8-plex iTRAQ proteomics of hippocampal synaptosomes isolated from *Ercc1*$^{\Delta/-}$ and wildtype littermates at 4 weeks (P28) and 16 weeks (P112) of age (Supplemental Figure S1) in order to identify whether quantitative changes in the proteome of hippocampal synapses may provide an explanation for the age-related behavioral deficits in *Ercc1*$^{\Delta/-}$ mice.[25] We confirmed the isolation of synaptosomes by showing enrichment of the synaptic protein marker PSD-95 (Supplemental Figure S2). For each time point, four independent *Ercc1*$^{\Delta/-}$ samples were compared with four independent wildtype samples. These four samples thus provide biological replicates and allow us to adequately test the reproducibility of our findings. All iTRAQ data are summarized in Supplemental Tables S1 and S2. We identified a total of 288 proteins with at least three peptides with a confidence interval >95%, and which were quantifiable by at least three peptides at each time point (Supplemental Table S3). SAM analysis indicated that the levels of 175 proteins were significantly different from wildtype controls at one or both time points (FDR <10) (Figure 3A; Supplemental Table S4). Most significant differentially expressed proteins were detected at P112 (148 proteins), whereas many fewer proteins showed differential expression at P28 (77 proteins). Fifty proteins showed significant differential expression at both time points. Thus, impaired DNA repair impacts heavily on the quantitative composition of the hippocampal synapses.

To confirm the iTRAQ results, we next performed quantitative immunoblotting (n = 6 per genotype) for a

dx.doi.org/10.1021/pr201203m | *J. Proteome Res.* 2012, 11, 1855–1867

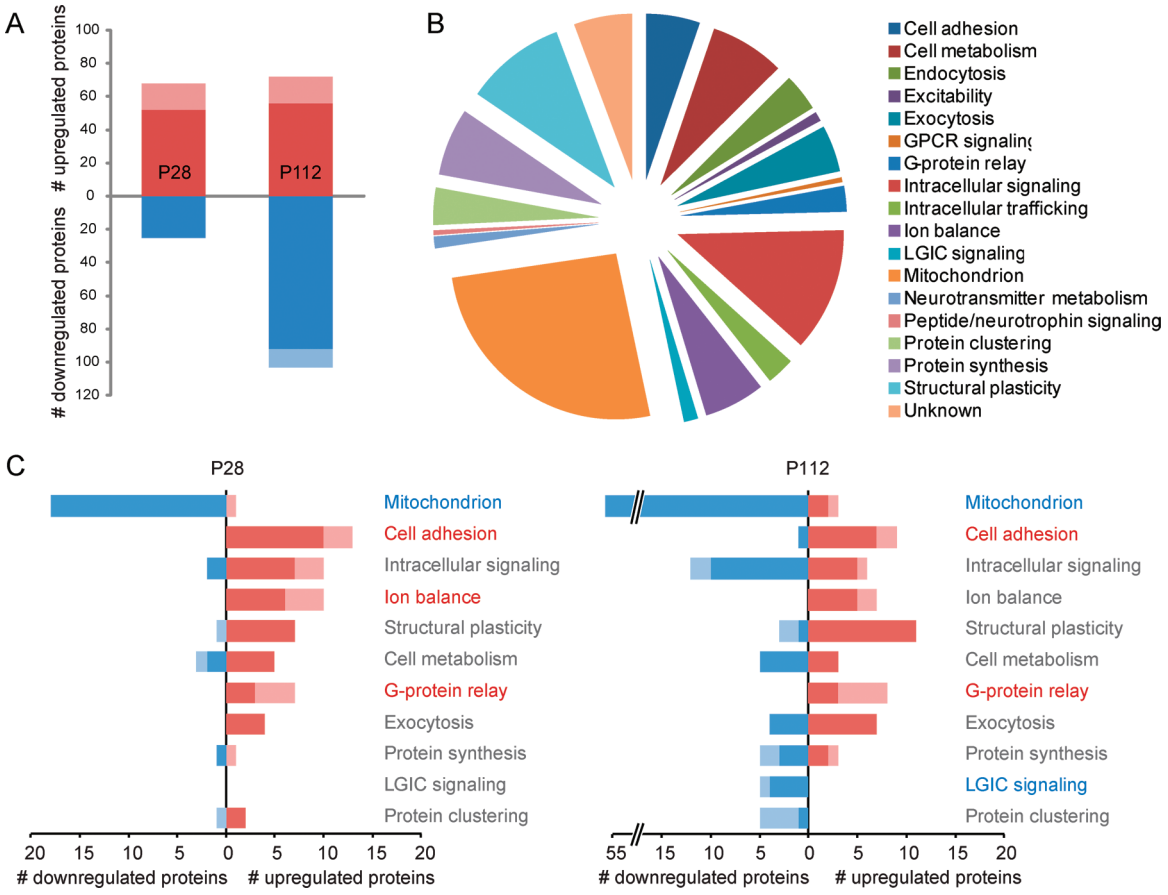

Figure 3. *Ercc1*$^{\Delta/-}$ mice show age-dependent changes in the proteomic composition of hippocampal synapses. (A) Bar graphs showing the number of significantly up- (red bars) and downregulated (blue bars) proteins at P28 and P112 (mutant relative to wildtype; FDR <10). Dark red and blue bars indicate protein numbers under stringent protein selection criteria; pale red and blue bars indicate protein numbers under relaxed protein selection criteria (see text for details). (B) Using relaxed protein selection criteria, a total of 439 proteins were detected, which could be assigned to 17 different functional protein groups. (C) Up- and downregulated proteins at either P28 (left panel) or P112 (right panel) were differentially enriched for several functional protein groups. Red and blue bars indicate the number of up- and downregulated proteins per functional group (dark red/blue, stringent protein selection criteria; pale red/blue, relaxed protein selection criteria). Functional protein group names indicated in bold are significantly enriched in the corresponding protein cluster using a Fisher's exact test (see also Table 1).

representative set of significant differentially expressed proteins (Figure 4). For proteins that were significantly regulated at P28, we confirmed the upregulation of neuromodulin (Gap43), neural cell adhesion molecule 1 (Ncam1), and Na,K-ATPase subunit beta-2 (Atp1b2) and the downregulation of calcium/calmodulin-dependent protein kinase II subunit alpha (Camk2a) (Figure 4A). For proteins that were significantly regulated at P112 we confirmed the upregulation of Gap43 and the downregulation of cytochrome *b*-c1 complex subunit 2 (Uqcrc2), AMPA-selective glutamate receptor subunit 1 (GluA1), and Camk2a (Figure 4B). These findings demonstrate that there is a perfect correlation between protein expression as measured by iTRAQ quantitative proteomics and by quantitative immunoblotting. In most cases, the changes in protein levels assessed by immunoblotting exceed the changes observed by iTRAQ, a phenomenon that was previously described in several other studies.[28,33]

Functional Characterization of Hippocampal Proteome Changes in *Ercc1*$^{\Delta/-}$ mice

To permit a large-scale functional interpretation of the overall changes in synaptic protein expression in *Ercc1* mutant mice, we also selected and quantified proteins using less stringent criteria. Instead of only including proteins with three or more quantifiable peptides at each time point, we now included all proteins with three or more quantifiable peptides at one time point and at least one quantifiable peptide at the other time point. By doing so, we reduce the risk of selectively discarding proteins that are less abundant at one time point, resulting in fewer detectable peptides at that time point. Using the relaxed protein selection criteria, a 52% increase in the total number of identifiable proteins was observed (439 compared to 288 using stringent selection; Supplemental Table S5). SAM analysis showed that the expression levels of 216 proteins were significantly different from those of wildtype controls at one or both time points (FDR <10) (Figure 3A; Table 1; Supplemental Table S6), which is 23% more than with stringent selection criteria. This modest increase in the number of differentially expressed proteins, together with the relatively strong increase in the number of detectable proteins, significantly increases the statistical power to detect changes in the overall expression of functional groups of protein.[33]

We next categorized all proteins in 17 functional synaptic protein groups as previously defined[37,38] (Figure 3B) and used a Fisher's exact test to determine which protein functions are significantly enriched within each of four protein clusters, i.e., proteins that are upregulated at P28, proteins that are downregulated at P28, proteins that are upregulated at P112,

dx.doi.org/10.1021/pr201203m | *J. Proteome Res.* 2012, 11, 1855–1867

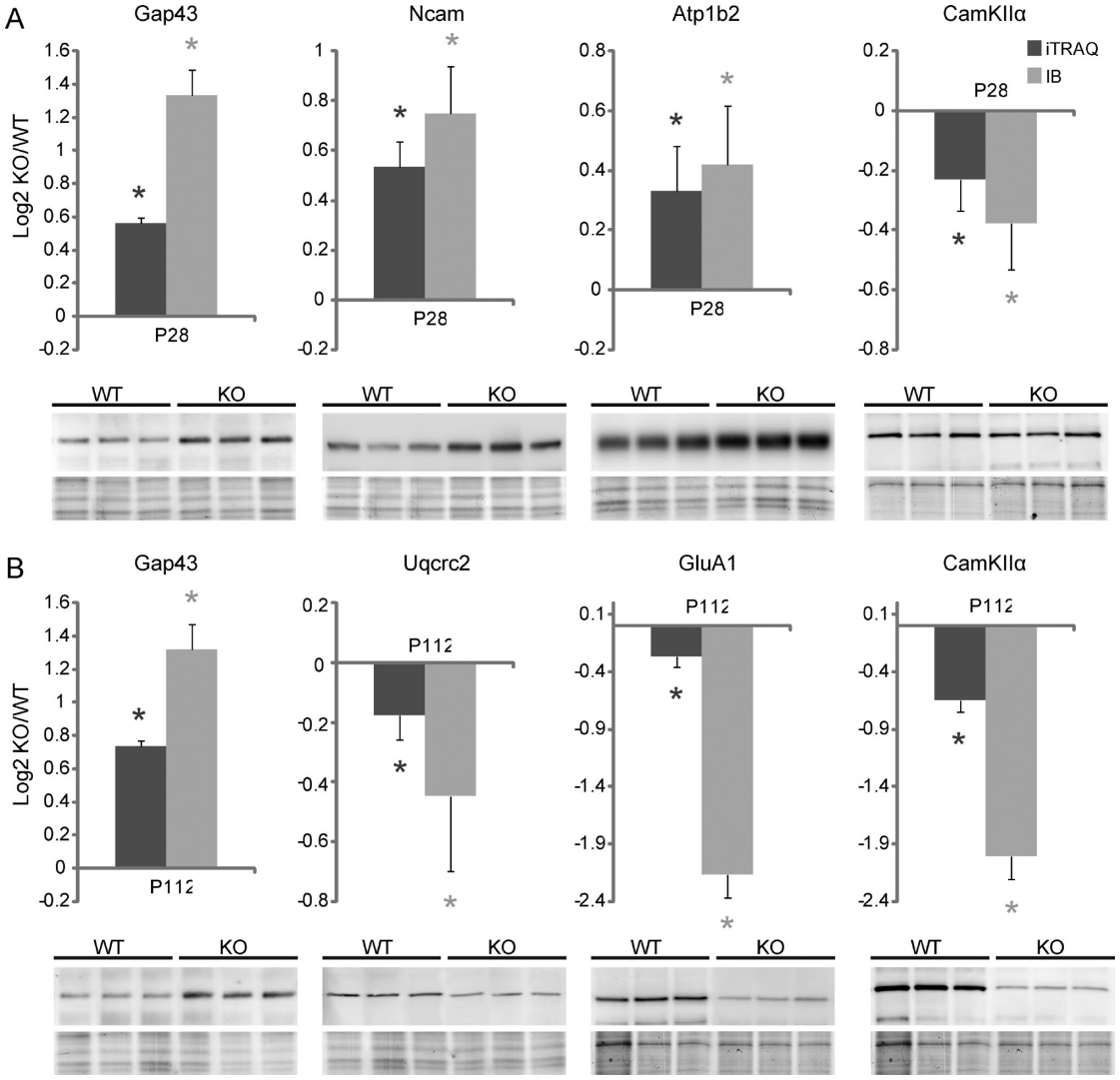

Figure 4. Validation of iTRAQ results by quantitative immunoblotting. (A) For proteins that were significantly regulated at P28, we confirmed the upregulation of neuromodulin (Gap43), neural cell adhesion molecule 1 (Ncam1), and Na,K-ATPase subunit beta-2 (Atp1b2) and the downregulation of calcium/calmodulin-dependent protein kinase II subunit alpha (Camk2a). (B) For proteins that were significantly regulated at P112, we confirmed the upregulation of Gap43 and the downregulation of cytochrome *b*-c1 complex subunit 2 (Uqcrc2), AMPA-selective glutamate receptor subunit 1 (GluA1), and Camk2a. *FDR <10 (iTRAQ) or $p < 0.05$ (immunoblot).

and proteins that are downregulated at P112 (Figure 3C; Table 2). The most significant enrichment was observed for mitochondrial proteins in downregulated protein clusters, both at P28 and at P112, with protein numbers increasing from 17 at P28 to 56 at P112. In addition, three protein functions were significantly enriched in upregulated proteins at P28, i.e., ion balance, cell adhesion, and G-protein relay. The latter two were also significantly enriched in upregulated proteins at P112. Finally, we observed a significant enrichment of proteins involved in ligand-gated ion channel (LGIC) signaling in downregulated proteins at P112. In particular, subunits of AMPA- and NMDA-type glutamate receptors were significantly downregulated at this time point. It is noteworthy that we observed a concomitant downregulation of several glutamate receptor-scaffolding proteins (protein clustering) and of several downstream intracellular signaling proteins. Although these last two functional groups were not significantly enriched, they do confirm that glutamate receptor signaling is indeed decreased at P112, but not yet at P28. Individual protein members of the above-mentioned functional groups (except mitochondrial protein) are listed in Figure 5, together with their levels of regulation at each time point. Taken together, our data show a significant and age-dependent deregulation of distinct synaptic protein signaling pathways during DNA damage-induced aging.

■ DISCUSSION

Ercc1 Mutant Mice As a Model for DNA Damage Induced Age-Related Synaptic Dysfunction

DNA damage plays an important role in aging.[6] Accumulation of DNA damage is associated with the age-dependent decline in vital functions,[40−42] and defects in genome maintenance are associated with accelerated aging in humans.[10−12] Thus, DNA is an important target of aging, and maintenance of genome integrity is a major anti-aging mechanism. Increasing evidence suggests that accumulation of DNA damage and subsequent genotoxic stress are also involved in aging of the brain[43−45] and that the inability of neurons to appropriately handle DNA damage may be causative in the etiology of neurodegenerative disorders.[46−49] As a model for accelerated brain aging we use

dx.doi.org/10.1021/pr201203m | *J. Proteome Res.* 2012, 11, 1855−1867

Table 1. Selection of Proteins That Are Significantly Regulated in Hippocampal Synapses of *Ercc1*$^{\Delta/-}$ Mice[a]

		log-fold change (KO/WT)		SAM FDR (%)		*t*-test *p*-value	
protein ID	gene symbol	P28	P122	P28	P112	P28	P112
G-Protein Relay							
GBG2_MOUSE	Gng2	0.49	0.16	0.0	18.1	0.003	0.157
GNAO_MOUSE	Gnao1	0.42	0.49	0.0	0.0	0.012	0.002
GBG7_MOUSE	Gng7	0.31	0.23	2.0	8.8	0.042	0.129
GNAZ_MOUSE	Gnaz	0.27	0.18	0.0	8.8	0.003	0.077
GNAS2_MOUSE	Gnas	0.20	0.21	0.0	1.8	0.002	0.014
GNA11_MOUSE	Gna11	0.20	0.05	5.5	42.2	0.060	0.579
GBB1_MOUSE	Gnb1	0.20	0.15	5.5	6.9	0.058	0.023
GNAI2_MOUSE	Gnai2	0.10	0.32	39.2	0.0	0.267	0.014
GNA13_MOUSE	Gna13	0.14	0.22	20.4	4.5	0.182	0.049
GNAI3_MOUSE	Gnai3	0.12	0.21	13.3	2.4	0.054	0.024
Ion Balance/Transport							
148707687	Atp2b4	0.61	0.13	0.0	22.8	0.002	0.151
AT1B1_MOUSE	Atp1b1	0.50	0.36	0.0	1.3	0.012	0.040
CXA1_MOUSE	Gja1	0.38	0.60	4.4	0.0	0.117	0.000
NAC1_MOUSE	Slc8a1	0.35	0.07	0.0	36.3	0.037	0.358
AT1B2_MOUSE	Atp1b2	0.33	0.19	1.7	25.5	0.067	0.296
AT1A1_MOUSE	Atp1a1	0.29	0.24	3.2	1.3	0.060	0.013
S12A5_MOUSE	Slc12a5	0.25	0.19	6.2	2.4	0.115	0.015
AT1A3_MOUSE	Atp1a3	0.23	0.37	5.5	1.1	0.090	0.027
S4A10_MOUSE	Slc4a10	0.21	0.06	4.1	33.8	0.045	0.168
VPP1_MOUSE	Atp6v0a1	0.16	−0.02	7.2	39.4	0.041	0.770
Cell Adhesion/Transsynaptic Signaling							
NCAM1_MOUSE	Ncam1	0.53	0.49	0.0	0.0	0.002	0.002
L1CAM_MOUSE	L1cam	0.45	0.33	0.0	1.4	0.001	0.032
CNTN1_MOUSE	Cntn1	0.37	0.32	0.0	0.0	0.007	0.016
GPM6A_MOUSE	Gpm6a	0.37	0.21	1.9	15.5	0.061	0.202
CD166_MOUSE	Alcam	0.36	0.39	0.0	0.0	0.001	0.018
NTRI_MOUSE	Ntm	0.33	0.14	0.0	24.9	0.036	0.218
GPM6B_MOUSE	Gpm6b	0.30	0.12	2.4	29.0	0.032	0.274
OX2G_MOUSE	Cd200	0.28	0.27	0.0	1.4	0.001	0.016
OMGP_MOUSE	Omg	0.22	0.25	3.0	1.3	0.033	0.020
TENR_MOUSE	Tnr	0.22	0.22	8.1	3.0	0.128	0.039
NFASC_MOUSE	Nfasc	0.15	0.19	8.2	1.3	0.053	0.003
IGSF8_MOUSE	Igsf8	0.15	0.23	4.1	1.1	0.005	0.005
NRX1A_MOUSE	Nrxn1	0.12	−0.12	6.2	14.2	0.005	0.201
148694008	Nptn	0.09	−0.15	46.9	6.5	0.455	0.055
LGIC Signaling							
GRIA2_MOUSE	Gria2	0.03	−0.14	52.9	8.3	0.644	0.074
NMDE2_MOUSE	Grin2b	0.07	−0.22	46.9	1.7	0.337	0.014
NMDZ1_MOUSE	Grin1	−0.05	−0.26	37.3	0.8	0.558	0.012
GRIA1_MOUSE	Gria1	−0.08	−0.26	33.3	1.7	0.436	0.028
NMDE1_MOUSE	Grin2a	0.08	−0.27	46.9	0.0	0.419	0.000

[a]Proteins that are involved in G-protein relay, ion balance, cell adhesion, and LGIC signaling and that are significantly regulated at one or both time points (using relaxed protein selection criteria) are listed, together with their associated log-fold change, FDR percentage, and *p*-value.

Ercc1 mutant mice. *Ercc1* mutant mice are indistinguishable from wildtype littermates at birth. However, they soon develop a severe and accelerated aging phenotype,[15,20−22] including progressive age-related neuropathological changes in the brain and the spinal cord and at neuromuscular junctions.[23] In a recent study, it was shown that hippocampal neurons in *Ercc1*$^{\Delta/-}$ mice show an age-dependent increase in the expression of several genotoxic markers, i.e., p53 and ATF3, compared with wildtype littermates, while very few neurons actually experienced cell death.[25] The authors conclude that between P28 and P112, neurons in the hippocampus of *Ercc1*$^{\Delta/-}$ mice become increasingly compromised due to genotoxic stress but do not die. Here we further substantiate these findings by showing that in addition to being healthy, cultured *Ercc1* mutant hippocampal neurons are capable of normal dendrite growth and synapse formation. Moreover, we did not observe differences in the gross dendritic morphology of the hippocampus or in the density of hippocampal dendritic spines between *Ercc1*$^{\Delta/-}$ mice and wildtype littermates at P112. In the literature, there is still controversy whether synapse loss actually contributes to early cognitive signs of aging.[50] In the *Ercc1* mutant mouse model, however, hippocampal synapse loss does not seem to be an important factor, allowing us to identify molecular changes at synapses that precede, or may even occur in the absence of, overt synapse loss.

dx.doi.org/10.1021/pr201203m | *J. Proteome Res.* 2012, 11, 1855−1867

Table 2. Significantly Enriched Functional Protein Classes within Protein Expression Clusters[a]

functional group	present in all detected proteins	present in cluster	Fisher's exact *p*-value
P28 Up			
cell adhesion	439/23	68/13	0.0003
G-protein relay	439/11	68/7	0.0054
ion balance	439/26	68/10	0.0184
P28 Down			
mitochondria	439/114	24/17	<0.0001
P112 Up			
cell adhesion	439/23	72/9	0.0312
G-protein relay	439/11	72/8	0.0022
P112 Down			
mitochondria	439/114	103/56	<0.0001
LGIC signaling	439/6	103/5	0.0397

[a]All quantified proteins were assigned to one of 17 functional synaptic protein groups. Up- and downregulated proteins at each time point (P28 and P112) were separately tested for overrepresentation of functional protein groups using a Fisher's exact test. Numerators represent the total number of proteins detected; denominators represent the number of proteins belonging to the indicated functional class.

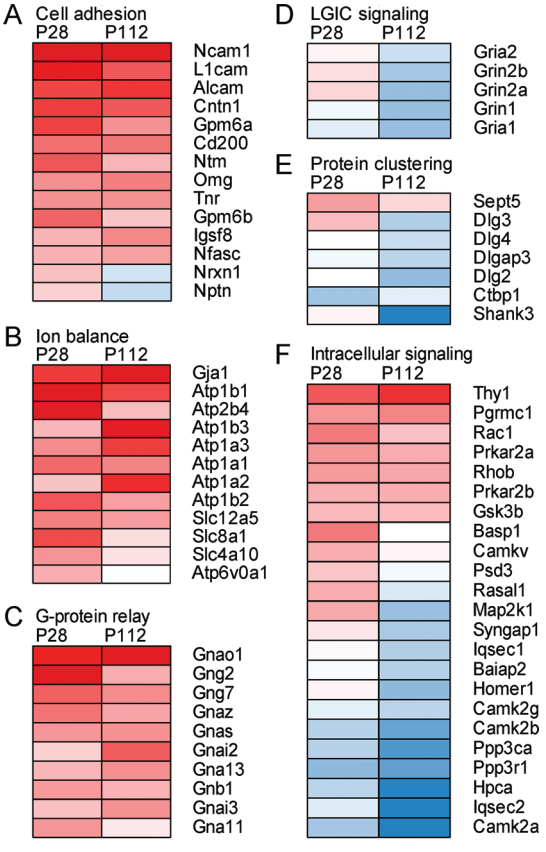

Figure 5. List of proteins that are significantly regulated in hippocampal synapses of *Ercc1*$^{\Delta/-}$ mice. Proteins that belong to the functional protein groups cell adhesion (A), ion balance (B), G-protein relay (C), LGIC signaling (D), protein clustering (E) and intracellular signaling (F) and that are significantly regulated at one or both time points (relaxed protein selection criteria) are indicated, together with their levels of regulation. Red indicates proteins that are upregulated; blue indicates proteins that are downregulated (mutant relative to wildtype).

Robust and Dynamic Changes in Synaptic Proteome Composition of *Ercc1* Mutant Mice

Quantitative proteomics revealed that the hippocampal synaptic proteome of *Ercc1*$^{\Delta/-}$ mice is very different from that of wildtype littermates. Depending on whether stringent or relaxed protein inclusion criteria were applied, 49–61% of all detected proteins showed significantly changed levels. These findings indicate that defective DNA repair as a result of the *Ercc1* mutation has a relatively large impact on synaptic protein composition.

Many changes in synaptic protein levels are age-specific, and we observed little overlap in significantly deregulated proteins at the two different time points that we investigated. Most changes in synaptic protein levels were observed at P112. This corresponds with the age at which *Ercc1*$^{\Delta/-}$ mice start to show reduced hippocampal long-term potentiation as well as clear deficits in spatial learning and memory.[25] Changes in synaptic protein levels at P112 may thus directly underlie physiological and behavioral alterations that are linked to age-related cognitive decline. At P28, on the other hand, no alterations in hippocampal synaptic plasticity and learning behavior are yet apparent.[25] Still, many synaptic proteins show significant changes in abundance at P28, and these changes are often specific for this early time point. It is tempting to speculate that these changes precede any significant physiological or behavioral deficits and that they thus may reflect early causative mechanisms in age-related cognitive decline (see below).

Early Proteomic Changes in *Ercc1* Mutant Synapses: Causative Factors for Cognitive Decline?

Synaptic proteins that are early affected in *Ercc1* mutant mice may play a causal role in the cognitive impairment observed later. Overrepresentation analysis of protein clusters that are either up- or downregulated at P28 revealed an enrichment of four distinct functional protein groups. Mitochondrial proteins were significantly enriched in downregulated proteins at P28. Mitochondrial dysfunction and the progressive decline in mitochondrial gene expression are conserved features of aging.[51,52] Moreover, age-related or toxin-induced mitochondrial dysfunction underlies neurodegenerative disorders, and it has been proposed that ROS-mediated mitochondrial defects may accumulate during and contribute to disease progression.[53] Finally, there is a causal and self-reinforcing link between mitochondrial dysfunction, ROS production, and DNA damage,[54] which may explain the lower synaptic expression of mitochondrial proteins in *Ercc1* mutant mice. Although on the basis of our proteomics data we cannot distinguish between differences in mitochondrial protein levels and overall mitochondrial abundance, our findings do confirm an important role for synaptic mitochondria during the early stages of brain aging.

Among upregulated proteins at P28, we observed a significant enrichment of proteins associated with ion balance. In particular, we found all subunits of the Na,K-ATPase complex to be more abundant in *Ercc1* mutant mice. Na,K-ATPase is a membrane-embedded sodium pump that functions to maintain the asymmetric distribution of sodium and potassium across the plasma membrane.[55] Sodium gradients form the foundation for synaptic transmission and neuronal excitation, and changes in the levels of Na,K-ATPases can cause long-term alterations in synaptic transmission.[56] Na,K-ATPases are also the primary energy consumers in the brain, utilizing half of the brains ATP content. Na,K-ATPases will therefore be

dx.doi.org/10.1021/pr201203m | *J. Proteome Res.* 2012, 11, 1855–1867

affected by decreased concentrations of ATP, caused by mitochondrial dysfunction, and the higher levels of Na,K-ATPases that we observed might be a compensatory mechanism to counteract the consequences of ATP depletion. We also found a significant enrichment of proteins involved in G-protein relay and in cell adhesion, both associated with upregulated proteins at P28. G-proteins are central relay factors between the activation of plasma membrane receptors by extracellular ligands, and the cellular responses that these ligands induce. In a recent large-scale gene linkage study, synaptic G-proteins were demonstrated to be significantly associated with cognitive ability (IQ).[37] In addition, several G-protein pathways have been implicated in the pathology of Alzheimer's disease.[57] Thus, early deregulation of synaptic G-proteins may well be an important contributing factor to age-dependent cognitive decline. Cell adhesion molecules may serve to facilitate both the organization and adhesion of the synapse. Dysfunction of cell adhesion molecules can lead to abnormalities in cell migration and synaptic plasticity and are found to be causal to cognitive impairments observed in, for instance, autism[58,59] and schizophrenia.[60,61] Whether early deregulation of these molecules also underlies age-dependent cognitive decline needs to be determined.

Late Proteomic Changes in *Ercc1* Mutant Synapses: Pathways for Permanent Cognitive Dysfunction?

Late affected synaptic proteins are more likely to be involved in the actual physiological changes underlying synaptic dysfunction and cognitive decline. Similarly as for P28, we observed a significant enrichment of mitochondrial proteins among downregulated proteins at P112 and of proteins involved in G-protein relay and in cell adhesion among upregulated proteins at P112, indicating that these represent sustained synaptic proteome changes in *Ercc1* mutant mice. A significant and age-specific enrichment was observed for proteins involved in LGIC signaling among downregulated proteins at P112. Interestingly, all five proteins in this functional group are ionotropic glutamate receptors, including the two major AMPA-type receptor subunits Gria1 and Gria2, which mediate fast excitatory transmission at hippocampal synapses, and the major NMDA-type receptor subunits Grin1, Grin2a, and Grin2b, which mediate calcium influx required for long-term changes in synaptic strength and are key to hippocampal learning and memory.[62] Interestingly, a concomitant downregulation of several proteins involved in protein clustering and intracellular signaling was observed. Although these functional protein groups were not significantly enriched using a Fisher's exact test, their individual protein members all show a significant downregulation in *Ercc1* mutant synapses at P112 specifically. Downregulated clustering proteins include Dlg2 (PSD-93), Dlg3 (SAP102), Dlg4 (Psd-95), Dlgap3, and Shank3, which are postsynaptic density proteins involved in the scaffolding of AMPA- and NMDA-type glutamate receptors.[63] Reduced abundance of these proteins in *Ercc1* mutant synapses at P112 thus reflects the inability of these synapses to correctly organize postsynaptic glutamate receptor signaling. Downregulated intracellular signaling proteins include three subunits of the calcium/calmodulin-dependent protein kinase type II complex (Camk2a, Camk2b, and Camk2g), both subunits of the calcium-dependent protein phosphatase calcineurin (Ppp3ca and Ppp3r1), and the calcium-binding protein Hpca (hippocalcin). These proteins all mediated calcium-dependent signaling downstream of

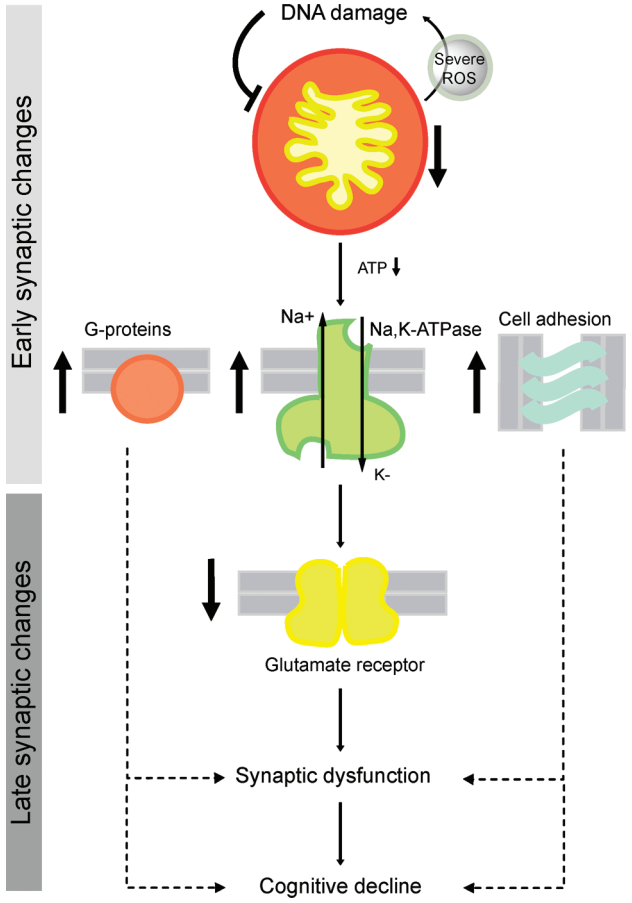

Figure 6. Synaptic proteins and cognitive decline: a hypothetical model. On the basis of our findings we propose the following model to explain DNA damage-induced aging and cognitive decline. Compromised DNA damage repair as in *Ercc1* mutants causes mitochondrial dysfunction. This then leads to increased levels of reactive oxygen species (ROS), which in turn causes further DNA damage and mitochondrial dysfunction. This self-reinforcing cycle of detrimental decline is central to normal and pathological aging.[54] Reduced mitochondrial activity or abundance also results in lowered concentrations of ATP, which in turn affects Na,K-ATPase function. The up-regulation of Na,K-ATPases that we observed could be a compensatory mechanism to counteract the effect of ATP depletion. Dysfunction of Na,K-ATPases is known to induce a rapid reduction in synaptic AMPA receptor surface expression and AMPA receptor protein abundance, leading to a long-lasting changes in synaptic function.[56] In addition to Na,K-ATPases, we found an early upregulation of proteins associated with G-protein relay and cell adhesion. Together, these early changes may lead to synaptic dysfunction and cognitive decline later in life.

NMDA receptors[64] and thus reflect reduced plasticity signaling in *Ercc1* mutant hippocampal glutamatergic synapses at P112. Importantly, Camk2 activation is regarded a master-switch for the induction of synaptic plasticity underlying learning and memory.[65]

Reduced expression of synaptic glutamate receptors and of synaptic glutamate receptor scaffolding and signaling components in *Ercc1*$^{\Delta/-}$ mice at P112 may well explain the deficits in hippocampal synaptic plasticity and learning behavior observed at this age.[25] These late changes in synaptic protein levels may however result from earlier changes, and establishing such causal relationships is important for defining molecular targets that may be used to pharmacologically treat and prevent

dx.doi.org/10.1021/pr201203m | J. Proteome Res. 2012, 11, 1855–1867

cognitive decline. In this respect it is interesting to note that Na,K-ATPase deregulation, as we observed at P28, is causally linked with glutamate receptor surface expression.[56] Na,K-ATPases are enriched at synapses and are co-localized and associated with ligand-gated ion channels such as AMPA receptors. Na,K-ATPase dysfunction induces a rapid reduction in AMPA receptor surface expression as well as total protein abundance, leading to a long-lasting depression of synaptic transmission.[56] As such Na,K-ATPase and mitochondrial dysfunction may well precede and possibly cause the observed glutamatergic signaling deficits.

CONCLUSIONS

A Model for Synaptic Dysfunction and Age-Related Cognitive Decline

In conclusion, we have provided a first comprehensive systems-level characterization of the temporal changes that occur in the synaptic proteome in a well-defined DNA repair deficient mouse model for aging. Our data implicate different synaptic signaling pathways in age-related synaptic dysfunction and lead to the following hypothetical model (Figure 6): (1) early downregulation of mitochondria causes ATP depletion, (2) ATP depletion leads to Na,K-ATPase dysfunction and a compensatory upregulation of Na,K-ATPase subunit expression, (3) dysfunction of Na,K-ATPases results in progressive downregulation of synaptic glutamate receptor expression and signaling, which causes long-term changes in synaptic function and cognitive impairment, and (4) other synaptic changes, including increased levels of G-proteins and cell adhesion proteins, may contribute to cognitive decline. Future experiments are required to determine how relevant these alterations are for human aging and, if so, whether targeted intervention of any of these pathways is able to improve cognitive function in aged humans.

ASSOCIATED CONTENT

Supporting Information

Supplemental Figure S1. Schematic representation of the 8-plex iTRAQ approach. **Supplemental Figure S2.** Enrichment of PSD-95 in hippocampal synaptosomes. **Supplemental Table S1.** Peptide identification and iTRAQ quantification information of set 1. **Supplemental Table S2.** Peptide identification and iTRAQ quantification information of set 2. **Supplemental Table S3.** All quantified proteins detected with stringent protein inclusion criteria: at least three unique peptides with a CI ≥ 95% and at least three peptides in all experiments identified. **Supplemental Table S4.** All significantly changed proteins detected with stringent protein inclusion criteria: at least three unique peptides with a CI ≥ 95%, at least three peptides in all experiments identified, and significant (FDR < 10%) at at least one time point. **Supplemental Table S5.** All quantified proteins detected with relaxed protein inclusion criteria: at least three unique peptides with a CI ≥ 95% and at least three peptides at one time point, and at least one quantifiable peptide at the other time point. **Supplemental Table S6.** All significantly changed proteins detected with relaxed protein inclusion criteria: at least three unique peptides with a CI ≥ 95% and at least three peptides at one time point, and at least one quantifiable peptide at the other time point, and significant (FDR < 10%) at at least one time point. This material is available free of charge via the Internet at http://pubs.acs.org.

AUTHOR INFORMATION

Corresponding Author

*Tel: +31 20 5987111. Fax: +31 20 5989281. E-mail: ronald.van.kesteren@cncr.vu.nl.

Author Contributions

§These authors contributed equally to this work.

Notes

The authors declare no competing financial interest.

ACKNOWLEDGMENTS

M.J.V. was supported by a Top Institute Pharma grant (T5-207). A.B.S., K.W.L., and R.E.v.K. received funding from the EU-FP7 framework Health program (SynSys; grant 242167). Additional support is acknowledged from EU-FP7 (MarkAge; grant 200880) and EU-FP6 (Lifespan; grant EC-LSHG-CT-2007-036894). The authors would like to thank Renata Brandt for technical assistance.

REFERENCES

(1) West, M. J.; Coleman, P. D.; Flood, D. G.; Troncoso, J. C. Differences in the pattern of hippocampal neuronal loss in normal ageing and Alzheimer's disease. *Lancet* **1994**, *344* (8925), 769−72.

(2) Rapp, P. R.; Gallagher, M. Preserved neuron number in the hippocampus of aged rats with spatial learning deficits. *Proc. Natl. Acad. Sci. U.S.A.* **1996**, *93* (18), 9926−30.

(3) Rasmussen, T.; Schliemann, T.; Sorensen, J. C.; Zimmer, J.; West, M. J. Memory impaired aged rats: no loss of principal hippocampal and subicular neurons. *Neurobiol. Aging* **1996**, *17* (1), 143−7.

(4) Keuker, J. I.; Luiten, P. G.; Fuchs, E. Preservation of hippocampal neuron numbers in aged rhesus monkeys. *Neurobiol. Aging* **2003**, *24* (1), 157−65.

(5) Burke, S. N.; Barnes, C. A. Neural plasticity in the ageing brain. *Nat. Rev. Neurosci.* **2006**, *7* (1), 30−40.

(6) Garinis, G. A.; van der Horst, G. T.; Vijg, J.; Hoeijmakers, J. H. DNA damage and ageing: new-age ideas for an age-old problem. *Nat. Cell Biol.* **2008**, *10* (11), 1241−7.

(7) O'Hagan, H. M.; Mohammad, H. P.; Baylin, S. B. Double strand breaks can initiate gene silencing and SIRT1-dependent onset of DNA methylation in an exogenous promoter CpG island. *PLoS Genet.* **2008**, *4* (8), e1000155.

(8) Loerch, P. M.; Lu, T.; Dakin, K. A.; Vann, J. M.; Isaacs, A.; Geula, C.; Wang, J.; Pan, Y.; Gabuzda, D. H.; Li, C.; Prolla, T. A.; Yankner, B. A. Evolution of the aging brain transcriptome and synaptic regulation. *PLoS One* **2008**, *3* (10), e3329.

(9) Lu, T.; Pan, Y.; Kao, S. Y.; Li, C.; Kohane, I.; Chan, J.; Yankner, B. A. Gene regulation and DNA damage in the ageing human brain. *Nature* **2004**, *429* (6994), 883−91.

(10) Bohr, V. A.; Wilson, D. M.; De Souza-Pinto, N. C.; van der Pluijm, I.; Hoeijmakers, J. H. J., DNA repair and aging. In *Molecular Biology of Aging*; Cold Spring Harbor Laboratory Press: New York, 2008; pp 309−46.

(11) Ramirez, C. L.; Cadinanos, J.; Varela, I.; Freije, J. M.; Lopez-Otin, C. Human progeroid syndromes, aging and cancer: new genetic and epigenetic insights into old questions. *Cell. Mol. Life Sci.* **2007**, *64* (2), 155−70.

(12) Schumacher, B.; van der Pluijm, I.; Moorhouse, M. J.; Kosteas, T.; Robinson, A. R.; Suh, Y.; Breit, T. M.; van Steeg, H.; Niedernhofer, L. J.; van Ijcken, W.; Bartke, A.; Spindler, S. R.; Hoeijmakers, J. H.; van der Horst, G. T.; Garinis, G. A. Delayed and accelerated aging share common longevity assurance mechanisms. *PLoS Genet.* **2008**, *4* (8), e1000161.

(13) Schumacher, B.; Garinis, G. A.; Hoeijmakers, J. H. Age to survive: DNA damage and aging. *Trends Genet.* **2008**, *24* (2), 77−85.

(14) Houtsmuller, A. B.; Rademakers, S.; Nigg, A. L.; Hoogstraten, D.; Hoeijmakers, J. H.; Vermeulen, W. Action of DNA repair

endonuclease ERCC1/XPF in living cells. *Science* **1999**, *284* (5416), 958−61.
(15) Niedernhofer, L. J.; Garinis, G. A.; Raams, A.; Lalai, A. S.; Robinson, A. R.; Appeldoorn, E.; Odijk, H.; Oostendorp, R.; Ahmad, A.; van Leeuwen, W.; Theil, A. F.; Vermeulen, W.; van der Horst, G. T.; Meinecke, P.; Kleijer, W. J.; Vijg, J.; Jaspers, N. G.; Hoeijmakers, J. H. A new progeroid syndrome reveals that genotoxic stress suppresses the somatotroph axis. *Nature* **2006**, *444* (7122), 1038−43.
(16) Ahmad, A.; Robinson, A. R.; Duensing, A.; van Drunen, E.; Beverloo, H. B.; Weisberg, D. B.; Hasty, P.; Hoeijmakers, J. H.; Niedernhofer, L. J. ERCC1-XPF endonuclease facilitates DNA double-strand break repair. *Mol. Cell. Biol.* **2008**, *28* (16), 5082−92.
(17) Zhu, X. D.; Niedernhofer, L.; Kuster, B.; Mann, M.; Hoeijmakers, J. H.; de Lange, T. ERCC1/XPF removes the 3′ overhang from uncapped telomeres and represses formation of telomeric DNA-containing double minute chromosomes. *Mol. Cell* **2003**, *12* (6), 1489−98.
(18) Bergstralh, D. T.; Sekelsky, J. Interstrand crosslink repair: can XPF-ERCC1 be let off the hook? *Trends Genet.* **2008**, *24* (2), 70−6.
(19) Bhagwat, N.; Olsen, A. L.; Wang, A. T.; Hanada, K.; Stuckert, P.; Kanaar, R.; D'Andrea, A.; Niedernhofer, L. J.; McHugh, P. J. XPF-ERCC1 participates in the Fanconi anemia pathway of cross-link repair. *Mol. Cell. Biol.* **2009**, *29* (24), 6427−37.
(20) McWhir, J.; Selfridge, J.; Harrison, D. J.; Squires, S.; Melton, D. W. Mice with DNA repair gene (ERCC-1) deficiency have elevated levels of p53, liver nuclear abnormalities and die before weaning. *Nat. Genet.* **1993**, *5* (3), 217−24.
(21) Weeda, G.; Donker, I.; de Wit, J.; Morreau, H.; Janssens, R.; Vissers, C. J.; Nigg, A.; van Steeg, H.; Bootsma, D.; Hoeijmakers, J. H. Disruption of mouse ERCC1 results in a novel repair syndrome with growth failure, nuclear abnormalities and senescence. *Curr. Biol.* **1997**, *7* (6), 427−39.
(22) Lawrence, N. J.; Sacco, J. J.; Brownstein, D. G.; Gillingwater, T. H.; Melton, D. W. A neurological phenotype in mice with DNA repair gene Ercc1 deficiency. *DNA Repair* **2008**, *7* (2), 281−91.
(23) de Waard, M. C.; van der Pluijm, I.; Zuiderveen Borgesius, N.; Comley, L. H.; Haasdijk, E. D.; Rijksen, Y.; Ridwan, Y.; Zondag, G.; Hoeijmakers, J. H.; Elgersma, Y.; Gillingwater, T. H.; Jaarsma, D. Age-related motor neuron degeneration in DNA repair-deficient Ercc1 mice. *Acta Neuropathol.* **2010**, *120* (4), 461−75.
(24) Nevedomskaya, E.; Meissner, A.; Goraler, S.; de Waard, M.; Ridwan, Y.; Zondag, G.; van der Pluijm, I.; Deelder, A. M.; Mayboroda, O. A. Metabolic profiling of accelerated aging ERCC1 d/- mice. *J. Proteome Res.* **2010**, *9* (7), 3680−7.
(25) Borgesius, N. Z.; de Waard, M. C.; van der Pluijm, I.; Omrani, A.; Zondag, G. C.; van der Horst, G. T.; Melton, D. W.; Hoeijmakers, J. H.; Jaarsma, D.; Elgersma, Y. Accelerated age-related cognitive decline and neurodegeneration, caused by deficient DNA repair. *J. Neurosci.* **2011**, *31* (35), 12543−53.
(26) Klychnikov, O. I.; Li, K. W.; Sidorov, I. A.; Loos, M.; Spijker, S.; Broos, L. A.; Frants, R. R.; Ferrari, M. D.; Mayboroda, O. A.; Deelder, A. M.; Smit, A. B.; van den Maagdenberg, A. M. Quantitative cortical synapse proteomics of a transgenic migraine mouse model with mutated Ca(V)2.1 calcium channels. *Proteomics* **2010**, *10* (13), 2531−5.
(27) Li, K. W.; Miller, S.; Klychnikov, O.; Loos, M.; Stahl-Zeng, J.; Spijker, S.; Mayford, M.; Smit, A. B. Quantitative proteomics and protein network analysis of hippocampal synapses of CaMKIIalpha mutant mice. *J. Proteome Res.* **2007**, *6* (8), 3127−33.
(28) Van den Oever, M. C.; Goriounova, N. A.; Li, K. W.; Van der Schors, R. C.; Binnekade, R.; Schoffelmeer, A. N.; Mansvelder, H. D.; Smit, A. B.; Spijker, S.; De Vries, T. J. Prefrontal cortex AMPA receptor plasticity is crucial for cue-induced relapse to heroin-seeking. *Nat. Neurosci.* **2008**, *11* (9), 1053−8.
(29) van Nierop, P.; Loos, M., Bioinformatics Procedures for Analysis of Quantitative Proteomics Experiments. In *Neuroproteomics*; Li, K. W., Ed.; Springer: New York, 2011; Vol. *57*.
(30) Tusher, V. G.; Tibshirani, R.; Chu, G. Significance analysis of microarrays applied to the ionizing radiation response. *Proc. Natl. Acad. Sci. U.S.A.* **2001**, *98* (9), 5116−21.
(31) Saeed, A. I.; Bhagabati, N. K.; Braisted, J. C.; Liang, W.; Sharov, V.; Howe, E. A.; Li, J.; Thiagarajan, M.; White, J. A.; Quackenbush, J. TM4 microarray software suite. *Methods Enzymol.* **2006**, *411*, 134−93.
(32) Mueller, R. S.; Denef, V. J.; Kalnejais, L. H.; Suttle, K. B.; Thomas, B. C.; Wilmes, P.; Smith, R. L.; Nordstrom, D. K.; McCleskey, R. B.; Shah, M. B.; Verberkmoes, N. C.; Hettich, R. L.; Banfield, J. F. Ecological distribution and population physiology defined by proteomics in a natural microbial community. *Mo.l Syst. Biol.* **2010**, *6*, 374.
(33) Dahlhaus, M.; Wan, Li, K.; van der Schors, R. C.; Saiepour, M. H.; van Nierop, P.; Heimel, J. A.; Hermans, J. M.; Loos, M.; Smit, A. B.; Levelt, C. N. The synaptic proteome during development and plasticity of the mouse visual cortex. *Mol. Cell. Proteomics* **2011**, *10* (5), M110 005413.
(34) Klemmer, P.; Meredith, R. M.; Holmgren, C. D.; Klychnikov, O. I.; Stahl-Zeng, J.; Loos, M.; van der Schors, R. C.; Wortel, J.; de Wit, H.; Spijker, S.; Rotaru, D. C.; Mansvelder, H. D.; Smit, A. B.; Li, K. W. Proteomics, ultrastructure, and physiology of hippocampal synapses in a fragile X syndrome mouse model reveal presynaptic phenotype. *J. Biol. Chem.* **2011**, *286* (29), 25495−504.
(35) Roxas, B. A.; Li, Q. Significance analysis of microarray for relative quantitation of LC/MS data in proteomics. *BMC Bioinf.* **2008**, *9*, 187.
(36) Counotte, D. S.; Li, K. W.; Wortel, J.; Gouwenberg, Y.; Van Der Schors, R. C.; Smit, A. B.; Spijker, S. Changes in molecular composition of rat medial prefrontal cortex synapses during adolescent development. *Eur. J. Neurosci.* **2010**, *32* (9), 1452−60.
(37) Ruano, D.; Abecasis, G. R.; Glaser, B.; Lips, E. S.; Cornelisse, L. N.; de Jong, A. P.; Evans, D. M.; Davey Smith, G.; Timpson, N. J.; Smit, A. B.; Heutink, P.; Verhage, M.; Posthuma, D. Functional gene group analysis reveals a role of synaptic heterotrimeric G proteins in cognitive ability. *Am. J. Hum. Genet.* **2010**, *86* (2), 113−25.
(38) Lips, E. S.; Cornelisse, L. N.; Toonen, R. F.; Min, J. L.; Hultman, C. M.; Holmans, P. A.; O'Donovan, M. C.; Purcell, S. M.; Smit, A. B.; Verhage, M.; Sullivan, P. F.; Visscher, P. M.; Posthuma, D. Functional gene group analysis identifies synaptic gene groups as risk factor for schizophrenia. *Mol. Psychiatry* **2011**.
(39) Testa, C. M.; Sherer, T. B.; Greenamyre, J. T. Rotenone induces oxidative stress and dopaminergic neuron damage in organotypic substantia nigra cultures. *Brain Res. Mol. Brain Res.* **2005**, *134* (1), 109−18.
(40) Hoeijmakers, J. H. DNA damage, aging, and cancer. *N. Engl. J. Med.* **2009**, *361* (15), 1475−85.
(41) Kirkwood, T. B. Understanding the odd science of aging. *Cell* **2005**, *120* (4), 437−47.
(42) Jackson, S. P.; Bartek, J. The DNA-damage response in human biology and disease. *Nature* **2009**, *461* (7267), 1071−8.
(43) Hamilton, M. L.; Van Remmen, H.; Drake, J. A.; Yang, H.; Guo, Z. M.; Kewitt, K.; Walter, C. A.; Richardson, A. Does oxidative damage to DNA increase with age? *Proc. Natl. Acad. Sci. U.S.A.* **2001**, *98* (18), 10469−74.
(44) Gedik, C. M.; Grant, G.; Morrice, P. C.; Wood, S. G.; Collins, A. R. Effects of age and dietary restriction on oxidative DNA damage, antioxidant protection and DNA repair in rats. *Eur. J. Nutr.* **2005**, *44* (5), 263−72.
(45) Dorszewska, J.; Adamczewska-Goncerzewicz, Z. Oxidative damage to DNA, p53 gene expression and p53 protein level in the process of aging in rat brain. *Respir. Physiol. Neurobiol.* **2004**, *139* (3), 227−36.
(46) Rass, U.; Ahel, I.; West, S. C. Defective DNA repair and neurodegenerative disease. *Cell* **2007**, *130* (6), 991−1004.
(47) Zhang, J.; Perry, G.; Smith, M. A.; Robertson, D.; Olson, S. J.; Graham, D. G.; Montine, T. J. Parkinson's disease is associated with oxidative damage to cytoplasmic DNA and RNA in substantia nigra neurons. *Am. J. Pathol.* **1999**, *154* (5), 1423−9.

(48) Mullaart, E.; Boerrigter, M. E.; Ravid, R.; Swaab, D. F.; Vijg, J. Increased levels of DNA breaks in cerebral cortex of Alzheimer's disease patients. *Neurobiol. Aging* **1990**, *11* (3), 169−73.
(49) Caldecott, K. W. Single-strand break repair and genetic disease. *Nat. Rev. Genet.* **2008**, *9* (8), 619−31.
(50) Lister, J. P.; Barnes, C. A. Neurobiological changes in the hippocampus during normative aging. *Arch. Neurol.* **2009**, *66* (7), 829−33.
(51) Yankner, B. A.; Lu, T.; Loerch, P. The aging brain. *Annu. Rev. Pathol.* **2008**, *3*, 41−66.
(52) Zahn, J. M.; Poosala, S.; Owen, A. B.; Ingram, D. K.; Lustig, A.; Carter, A.; Weeraratna, A. T.; Taub, D. D.; Gorospe, M.; Mazan-Mamczarz, K.; Lakatta, E. G.; Boheler, K. R.; Xu, X.; Mattson, M. P.; Falco, G.; Ko, M. S.; Schlessinger, D.; Firman, J.; Kummerfeld, S. K.; Wood, W. H. 3rd; Zonderman, A. B.; Kim, S. K.; Becker, K. G. AGEMAP: a gene expression database for aging in mice. *PLoS Genet.* **2007**, *3* (11), e201.
(53) Lin, M. T.; Beal, M. F. Mitochondrial dysfunction and oxidative stress in neurodegenerative diseases. *Nature* **2006**, *443* (7113), 787−95.
(54) Bishop, N. A.; Lu, T.; Yankner, B. A. Neural mechanisms of ageing and cognitive decline. *Nature* **2010**, *464* (7288), 529−35.
(55) Kaplan, J. H. Biochemistry of Na,K-ATPase. *Annu. Rev. Biochem.* **2002**, *71*, 511−35.
(56) Zhang, D.; Hou, Q.; Wang, M.; Lin, A.; Jarzylo, L.; Navis, A.; Raissi, A.; Liu, F.; Man, H. Y. Na,K-ATPase activity regulates AMPA receptor turnover through proteasome-mediated proteolysis. *J. Neurosci.* **2009**, *29* (14), 4498−511.
(57) Thathiah, A.; De Strooper, B. The role of G protein-coupled receptors in the pathology of Alzheimer's disease. *Nat. Rev. Neurosci.* **2011**, *12* (2), 73−87.
(58) Kim, H. G.; Kishikawa, S.; Higgins, A. W.; Seong, I. S.; Donovan, D. J.; Shen, Y.; Lally, E.; Weiss, L. A.; Najm, J.; Kutsche, K.; Descartes, M.; Holt, L.; Braddock, S.; Troxell, R.; Kaplan, L.; Volkmar, F.; Klin, A.; Tsatsanis, K.; Harris, D. J.; Noens, I.; Pauls, D. L.; Daly, M. J.; MacDonald, M. E.; Morton, C. C.; Quade, B. J.; Gusella, J. F. Disruption of neurexin 1 associated with autism spectrum disorder. *Am. J. Hum. Genet.* **2008**, *82* (1), 199−207.
(59) Jamain, S.; Quach, H.; Betancur, C.; Rastam, M.; Colineaux, C.; Gillberg, I. C.; Soderstrom, H.; Giros, B.; Leboyer, M.; Gillberg, C.; Bourgeron, T. Mutations of the X-linked genes encoding neuroligins NLGN3 and NLGN4 are associated with autism. *Nat. Genet.* **2003**, *34* (1), 27−9.
(60) Walsh, T.; McClellan, J. M.; McCarthy, S. E.; Addington, A. M.; Pierce, S. B.; Cooper, G. M.; Nord, A. S.; Kusenda, M.; Malhotra, D.; Bhandari, A.; Stray, S. M.; Rippey, C. F.; Roccanova, P.; Makarov, V.; Lakshmi, B.; Findling, R. L.; Sikich, L.; Stromberg, T.; Merriman, B.; Gogtay, N.; Butler, P.; Eckstrand, K.; Noory, L.; Gochman, P.; Long, R.; Chen, Z.; Davis, S.; Baker, C.; Eichler, E. E.; Meltzer, P. S.; Nelson, S. F.; Singleton, A. B.; Lee, M. K.; Rapoport, J. L.; King, M. C.; Sebat, J. Rare structural variants disrupt multiple genes in neurodevelopmental pathways in schizophrenia. *Science* **2008**, *320* (5875), 539−43.
(61) Kirov, G.; Gumus, D.; Chen, W.; Norton, N.; Georgieva, L.; Sari, M.; O'Donovan, M. C.; Erdogan, F.; Owen, M. J.; Ropers, H. H.; Ullmann, R. Comparative genome hybridization suggests a role for NRXN1 and APBA2 in schizophrenia. *Hum. Mol. Genet.* **2008**, *17* (3), 458−65.
(62) Kullmann, D. M.; Lamsa, K. P. Long-term synaptic plasticity in hippocampal interneurons. *Nat. Rev. Neurosci.* **2007**, *8* (9), 687−99.
(63) Kim, E.; Sheng, M. PDZ domain proteins of synapses. *Nat. Rev. Neurosci.* **2004**, *5* (10), 771−81.
(64) Lee, Y. S.; Silva, A. J. The molecular and cellular biology of enhanced cognition. *Nat. Rev. Neurosci.* **2009**, *10* (2), 126−40.
(65) Lisman, J.; Schulman, H.; Cline, H. The molecular basis of CaMKII function in synaptic and behavioural memory. *Nat. Rev. Neurosci.* **2002**, *3* (3), 175−90.